Research Square

Preprints are preliminary reports that have not undergone peer review.
They should not be considered conclusive, used to inform clinical practice,
or referenced by the media as validated information.

Annexin A1-Mediated Therapeutic Effect of Extracellular Vesicles Derived from Thrombin-Preconditioned Mesenchymal Stromal Cells in Experimental Necrotizing Enterocolitis

Choleun Kwon
SAIHST, Sungkyunkwan University
Sein Hwang
SAIHST, Sungkyunkwan University
Young Eun Kim
Samsung Medical Center
Misun Yang
Samsung Medical Center
So Yoon Ahn
Samsung Medical Center
Se In Sung
Samsung Medical Center
Yun Sil Chang
yschang@skku.edu

Samsung Medical Center

Research Article

Keywords: necrotizing enterocolitis, mesenchymal stromal cells, extracellular vesicle, Annexin A1, multi-omics

Posted Date: November 6th, 2026

DOI: https://doi.org/10.21203/rs.3.rs-10911604/v1

License: This work is licensed under a Creative Commons Attribution 4.0 International License.
Read Full License

Additional Declarations: No competing interests reported.

Abstract

Background

Necrotizing enterocolitis (NEC) is a devastating inflammatory disease in premature infants lacking specific treatment. Extracellular vesicles from thrombin-preconditioned mesenchymal stromal cells (thMSC-EVs) show enhanced therapeutic efficacy over naïve MSC-EVs. This study aimed to identify the key enriched therapeutic factor and its mechanism in experimental NEC.

Methods

Comparative proteomic profiling (LC-MS/MS) of thMSC-EVs was performed to identify candidate proteins. NEC was induced in neonatal mice (P4) using formula feeding, LPS, and stress. thMSC-EVs were administered intraperitoneally. Bulk RNA-sequencing and multi-omics ligand-receptor analyses of the mouse ileum integrated proteomic and transcriptomic data. The candidate, Annexin A1, was validated using in vitro LPS-induced inflammation and multiple-hit (HIT) models, assessing viability, barrier integrity, and NF-κB and Wnt/β-catenin signaling following treatment with thMSC-EVs, the Annexin A1 mimetic peptide (Ac2-26), and ANXA1-knockdown MSC-derived EVs (siANXA1-MSC-EVs).

Results

Proteomic analysis showed thMSC-EVs were significantly enriched with anti-inflammatory proteins, including a 3.8-fold increase in ANXA1. In the NEC model, thMSC-EVs attenuated intestinal necrosis and apoptosis, suppressed the mucosal antimicrobial response, and promoted tissue repair. Multi-omics ligand-receptor analysis identified the Annexin A1–formyl peptide receptor 1 interaction as the most prominent therapeutic axis. In vitro, Ac2-26 replicated the effects of thMSC-EVs, restoring cell viability and ZO-1 expression and suppressing NF-κB while restoring Wnt/β-catenin signaling. Conversely, siANXA1-MSC-EVs showed a significantly, though partially, diminished therapeutic effect.

Conclusion

Thrombin preconditioning amplifies the ANXA1 content within MSC-EVs. This enriched ANXA1 exerts a dual therapeutic effect in NEC by suppressing TLR4/NF-kB-mediated inflammation and promoting Wnt/β-catenin-mediated epithelial regeneration via the FPR signaling. Our findings establish ANXA1 as a major, though not exclusive, effector of thMSC-EVs and as a novel therapeutic target for NEC, supporting thMSC-EVs as a potent cell-free therapeutic agent.

Introduction

Necrotizing enterocolitis (NEC) is a high-mortality inflammatory and ischemic bowel disorder that predominantly affects premature infants in the neonatal intensive care unit, which frequently require bowel resection, resulting in subsequent short bowel syndrome and impaired long-term neurodevelopment [1–6]. Despite advances in neonatal care, the global incidence remains approximately 7% among premature infants, with a mortality rate averaging 20% [7, 8]. The absence of specific, disease-ameliorating therapies for NEC underscores the urgent clinical need for regenerative treatment, that can both suppress inflammation and restore intestinal integrity [9, 10].

The pathogenesis of NEC is characterized by a synergistic combination of two pathological features: excessive mucosal inflammation and defective epithelial regeneration [9, 11–13]. The immature intestine exhibits an exaggerated immune response mediated by the Toll-like Receptor 4 (TLR4) and the downstream nuclear factor kappa-light-chain-enhancer of activated B cells (NF-κB) pathway in response to pathogen-associated molecular patterns (PAMPs) like lipopolysaccharide (LPS) [9, 14–17]. This inflammatory cascade not only drives inflammation but also suppresses the Wingless/Integrated (Wnt)/β-catenin pathway, which is essential for intestinal stem cell maintenance and epithelial repair [16, 18–20]. Because injury and failed repair are mechanistically coupled in this way, an effective NEC therapeutic must simultaneously restrain the inflammatory drive and restore the regenerative capacity of the crypt.

Mesenchymal stromal cells (MSCs) have emerged as a promising therapeutic for NEC, owing to their anti-inflammatory and regenerative properties [21–27]. Recent studies have revealed that the therapeutic effects of MSCs is mediated by their secreted extracellular vesicles (EVs), which are membrane-bound vesicles that carry bioactive proteins, lipids, and RNAs [28, 29]. For neonatal application, EVs can offer additional advantages over MSCs, including cell-free nature, reduced immunogenicity, and improved stability as an “off-the-shelf” therapeutic [28, 30]. To augment the regenerative and anti-inflammatory properties of MSCs and their EVs, diverse priming or preconditioning strategies have been introduced [31, 32]. Among these, thrombin preconditioning exposes MSCs to a hemorrhagic injury-mimicking environment and, acting through protease-activated receptor (PAR)-mediated signaling, boosts both EV biogenesis and the enrichment of therapeutic cargo [30–32]. We considered this stimulus particularly relevant to NEC, since hemorrhagic lesions are a recognized component of NEC intestinal pathology [10]. Since modulation of MSCs alters the composition of molecules secreted into their EVs, we previously confirmed that thrombin-preconditioned MSCs’ derived EVs (thMSC-EVs) boost their cargo contents and thereby enhance their therapeutic effect in the experimental necrotizing enterocolitis model compared to naïve MSC-EVs [33]. We have also observed consistent benefits of thMSCs and their EVs in neonatal brain and lung disorder models [34–36], which suggests a shared molecular effector rather than an organ-specific one.

Our previous work, however, established only that thMSC-EVs are efficacious and that their cargo is broadly enriched in anti-apoptotic, anti-inflammatory, cell adhesion, and Wnt signaling annotations; no individual mediator was nominated, and no downstream pathway was tested [33]. This left the central question of EV: which of their many constituents does the work, and through which receptor. Therefore,

we hypothesized that the enhanced therapeutic efficacy of thMSC-EVs may stem from the selective enrichment of bioactive proteins capable of simultaneously attenuating inflammation and promoting epithelial regeneration. This study aimed to identify the key therapeutic mediator within thMSC-EVs by employing an integrative multi-omics approach that combined the EV proteomics with the intestinal transcriptomics of the thMSC-EVs administered NEC mouse model, reasoning that a cargo ligand enriched by thrombin and matched to a receptor transcriptionally induced by injury would be the most probable mediator. The nominated candidate was then interrogated in two directions that the omics analysis alone cannot address: sufficiency, by delivering the molecule alone as a mimetic peptide, and necessity, by depleting it from the EVs at source.

Methods

Ethics statement

All procedures involving human cells and animals were reviewed and approved by the institution. Human Wharton's Jelly-derived MSCs (WJ-MSCs) were obtained from the Samsung Medical Center's Good Manufacturing Practice (GMP) Facility. The obtained WJ-MSCs was established from a single donor with informed consent under Samsung Medical Center's Institutional Review Board (IRB) approval (IRB approval number: 2016-07-102-043). The Institutional Animal Care and Use Committee (IACUC) of the Research Institute for Future Medicine (RIFM) at Samsung Medical Center approved all animal protocols (IRB approval numbers 20231115001 and 20230116001). The RIFM is an AAALAC International-accredited institution, and all animal care followed the Institute of Laboratory Animal Resources guide. The animal study was performed in accordance with ARRIVE guidelines, and euthanasia was conducted following the 2020 AVMA Guidelines. All studies were conducted within the study period indicated in the IRB.

Production and characterization of MSC-Derived extracellular vesicles

EVs were generated from WJ-MSCs at passage 7, according to the previously established protocol [33]. WJ-MSCs were cultured following the minimum criteria of the International Society for Cell Therapy, confirmed for MSC markers by Western blot, and were subjected to a thrombin preconditioning protocol as previously detailed [36]. In short, thMSCs were produced by incubating WJ-MSCs for 3 hours in serum-free MEMα medium containing 20 units/mL of thrombin (Reyon Pharmaceutical Co., Ltd., Seoul, South Korea). Naïve MSCs were produced in the same serum-free medium but without thrombin. To isolate EVs, the conditioned media were collected and processed via tangential flow filtration (TFF) using a KrosFlo® KR2i system (Repligen; Waltham, MA, USA) equipped with a 300-kDa mPES membrane to concentrate EVs in diluent DPBS (Welgene, Daegu, South Korea). The EVs used in this study were from the same batches and lots characterized for particle concentration, size distribution, and surface

markers according to the MISEV guidelines in our previous study [29, 33]. Final EV suspensions were adjusted to a concentration of 2 × 10^{10} particles/mL and cryopreserved at -80°C for further use.

Extracellular vesicle proteomics and ligand–receptor interaction analysis

The comparative proteomic profile of naïve and thMSC-EVs was initially generated and reported in our previous study [33]. The previous study only presented the differences in Gene Ontology (GO) enrichment between the thMSC-EVS and naïveMSC-EVs, without depicting a therapeutic candidate or fully elucidating the therapeutic mechanism. In this study, the raw LC MS/MS data were analyzed in R studio and CellTalkDB database [37]. Proteins were classified as shared or unique between naïveMSC-EVs and thMSC-EVs by detection, and for each shared protein the relative abundance in thMSC-EVs versus naïveMSC-EVs was expressed as a log2 fold change. Proteins annotated as secreted ligands in the CellTalkDB database were retained for ligand–receptor analysis. Since the EV proteome was human origin whereas the tissue transcriptome was murine origin, human gene symbols were mapped to their mouse orthologs using the babelgene R package, and the analysis was performed against Mus musculus CellTalkDB ligand–receptor reference. At present, no database directly integrates ligand–receptor annotations across species. For each annotated ligand–receptor pair, an interaction score was calculated as the difference between the log2 fold change ligand enrichment in thMSC-EVs compared to naïveMSC-EV and the log2 fold expression of the receptor in the CON, NEC, and NEC+thEV groups. Pairs in which the ligand was enriched in thMSC-EVs, the receptor was induced in NEC, and the receptor induction was statistically significant ($P < 0.05$) were prioritized, yielding the ranked interactions reported in Fig. 2B.

In vivo NEC model

Animal study was conducted in line with the ARRIVE guidelines 2.0, and the inclusion and exclusion criteria were established a priori. An experimental model of NEC was established in postnatal day 4 (P4) ICR mouse pups, following the protocol based on previous study [33]. A cage of litters included 14 pups with a surrogate dam. Briefly, pups with body weight between 2.5g to 3.0g were randomly subjected to healthy normal control (CON), NEC control (NEC), and thMSC-EV-treated NEC (NEC+thEV) groups. Each experimental set consisted of approximately 4, 10, and 10 pups in CON, NEC, and NEC + thEV groups, respectively. Pups were subjected to a daily regimen of stressors for three consecutive days, consisting of three cycles per day. Each cycle involved oral administration of 60 µg LPS, gavage feeding with 100 µL of hyperosmolar formula (prepared by adding formula powder to Esbilac puppy milk), a 10-minute exposure to hypothermia (4°C), and a 20-minute exposure to hypoxia (5% O_2, 95% N_2). Immediately following the first stress cycle each day, pups in the treatment group received an intraperitoneal (IP) injection of thMSC-EVs (2 × 10^9 particles in 100 µL), a dosage informed by prior NEC studies [33]. The NEC group received 100 µL of PBS via IP injection. A dam-fed group served as the normal control. The researcher was aware of the group allocation during the injection, since the same treatment must be

administered throughout the experiment. Body weight and survival were monitored on a daily basis, and only those pups that survived throughout the entire duration of the study were incorporated into the final analysis. To minimize potential confounders arising from the order of treatment, the order of saline or thMSC-EV injection was randomly selected. At P7, a clinical sickness score was assigned by a blinded investigator based on a modified rubric [38], after which the animals were euthanized for tissue collection. Euthanasia was performed according to the American Veterinary Medical Association (AMVA) Guidelines for the Euthanasia of Animals (2020). P7 mouse pups were euthanized in a closed chamber using a lethal dose of isoflurane (Hana Parm Co., LTD; Seoul, South Korea). Dams were euthanized using a CO_2 euthanasia chamber, followed by a cervical dislocation. No animals were excluded from the analysis due to pre-established exclusion criteria, such as significant weight loss.

In vitro NEC models

Two in vitro models were used to simulate NEC pathology: multifactorial epithelial stress, and immune-mediated epithelial damage [33]. For the multiple-hit (HIT) model, the rat intestinal epithelial cell line IEC-6 (ATCC) was subjected to a combination of stressors for 24 hours: hyperosmolarity (1% DSS), ischemia (glucose-free medium), hypothermia (32°C), and hypoxia (1% O_2) (28–30). For the inflammatory model, primary peritoneal macrophages (PMs) were harvested from P11 Sprague-Dawley rats. Following a 24-hour stabilization period, these cells were activated with 0.1 μg/mL LPS (O111:B4; Sigma Aldrich; Burlington, MA, USA) for 24 hours. The resulting conditioned medium (CM) was collected for subsequent experiments.

Annexin A1 mimetic peptide

To investigate the effects of Annexin A1, its mimetic peptide Ac2-26 (HY-P1098; MedChemExpress, Monmouth Junction, NJ, USA) was used in vitro. Ac2-26 (3 μM) was treated to the in vitro HIT and inflammatory models.

siRNA-mediated Annexin A1 knockdown

WJ-MSCs were transfected with ANXA1-targeting siRNA (Bioneer, Daejeon, South Korea) or a negative control scrambled siRNA using the Neon Transfection System (MPK10096; Invitrogen, Carlsbad, CA, USA). Following transfection, WJ-MSCs were stabilized for 48 hours before the medium was replaced with thrombin-supplemented serum-free medium. After another 24 hours with or without thrombin-preconditioning, the conditioned medium was collected, and EVs were harvested using Amicon Ultra-15 Centrifugal Filter Units (Merck Millipore, UFC910024) by centrifugation at 4000 x g for 20 minutes. Since TFF requires at least 500 mL of conditioned medium to isolate EVs, Amicon was used to produce a lab-scale amount of knockdown EVs. Knockdown was confirmed by RT-qPCR and ELISA.

Bulk RNA sequencing and transcriptomic analysis

Total RNA was extracted from the ileal tissues of CON, NEC, and NEC+thEV groups (n = 3,5,5 per group, respectively) by Macrogen (Seoul, South Korea), where library preparation, Illumina sequencing, and alignment to the mouse reference genome were performed. Libraries were prepared and sequenced on an Illumina platform. Per-gene read counts were returned for downstream analysis. All subsequent analysis was performed in R. Differential expression between groups was assessed with DESeq2 using the Wald test, with genes considered differentially expressed at an adjusted $P < 0.05$ and $|\log2 \text{ fold change}| > 1$. For unsupervised analysis, counts were variance-stabilized and principal component analysis was performed on the top 500 most variable genes. Differentially expressed genes (DEGs) were grouped by the experimental group in which they were most enriched, and Gene Ontology biological process (GO-BP) enrichment across these groups was performed and visualized using the compareCluster function of clusterProfiler. Group-level comparisons of individual genes were made on variance-stabilized values by one-way ANOVA with Tukey's post-hoc test.

Integrated Multi-Omics Ligand-Receptor Interaction Analysis

To predict potential signaling axis, the list of ligands from the thMSC-EVs proteomic data was integrated with the list of receptors from the intestinal transcriptomic data. CellChat database was used to analyze ligand-receptor analysis in NEC+thEV group transcriptomics and thMSC-EVs proteomics [39]. The interaction strength of ligand-receptor pairs in each experimental group was calculated using the database to identify signaling pathways significantly activated by thMSC-EV treatment.

Histological Analysis

For histological examination, ileal tissues were fixed in 4% paraformaldehyde, processed into paraffin blocks using a swiss-roll technique, and sectioned at 4 μm. For histological examination, ileal segments were immediately swiss-rolled and fixed in 4% paraformaldehyde before being embedded in paraffin blocks to allow for precise longitudinal sectioning. Embedded tissues were sectioned into 4μm thick slides, and sections exhibiting the full longitudinal orientation of the villi were selected for staining. The severity of NEC-induced intestinal injury was quantified using a modified histological damage scoring system. Images were captured under 20times magnification and scored according to the following criteria: Grade 0: Intact villi with eosinophilic cytoplasm; Grade 1: Intact villi exhibiting pale cytoplasm; Grade 2: Loss of villi with pale cytoplasm; and Grade 3: Severe sloughing of villi resulting in areas denuded of epithelium. For all histological analyses, a single investigator blinded to the experimental groups scored a minimum of six images taken from each histological slide. Apoptosis was detected in tissue sections using a DeadEnd™ Fluorometric TUNEL System (Promega, Madison, WI, USA) according to the manufacturer's protocol (33). For immunofluorescent staining, sections underwent antigen retrieval and were incubated overnight at 4°C with primary antibodies against.

Biochemical Analysis

In vitro cell viability was assessed using a CCK-8 assay kit (Dojindo laboratory; Kumamoto, Japan). Protein extracts were separated by SDS-PAGE, transferred to nitrocellulose membranes, and probed with primary antibodies against AKT(1:1000, 9272; Cell Signaling Technology, Danvers, MA, USA), p-AKT(1:1000, D9E; Cell Signaling Technology, Danvers, MA, USA), NF-κB(1:1000, D14E12; Cell Signaling Technology, Danvers, MA, USA), β-catenin(1:1000; Abcam, ab6302, Cambridge, UK), p-GSK3β(1:1000, D85E12; Cell Signaling Technology, Danvers, MA, USA), ZO-1 (1:1000, 40-2200; Invitrogen, Carlsbad, CA, USA) and GAPDH (1:1000; Santa Cruz, Dallas, TX, USA), followed by chemiluminescent detection using Amersham ECL reagents (Cytvia, Marlborough, MA, USA). Anti-Ki67 was used for immunocytochemistry to quantify proliferating cells (PA5-19462; Invitrogen, Carlsbad, CA, USA). The level of human Annexin A1 was measured using ELISA kit following the manufacturer's protocol (ab222868; Abcam, Cambridge, UK). The pro-inflammatory cytokines (IL-1α, IL-1β, IL-6, TNFα) were measured using an ELISA kit following the manufacturer's protocol (LXSAMSM-04; R&D Systems, Minneapolis, MN, USA).

Statistical Analysis

All experimental results are expressed as the mean ± standard error of the mean (SEM). Comparisons between groups were made using one-way analysis of variance (ANOVA) followed by Tukey's or Bonferroni's post-hoc test, or the non-parametric Mann-Whitney U test where appropriate. Gene-level differential expression used the DESeq2 Wald test with Benjamini–Hochberg adjustment. Analyses were performed using GraphPad Prism 8.0 software (GraphPad, San Diego, CA, USA) or R. A P-value of less than 0.05 was considered statistically significant.

Results

thMSC-EV administration attenuated cell death and tissue necrosis and partially reversed the injury-associated transcriptome in vivo.

Consistent with our previous study [33], the induced tissue necrosis and cell death induced in the NEC group, assessed by histological damage score and TUNEL assay, respectively, were significantly ameliorated in the NEC+thEV group compared to the NEC group (Fig. 1A). Repeated GI-protective effects of thMSC-EVs in the experimental NEC model prompted us to investigate the underlying mechanism.

Bulk-seq was performed on FFPE ileal samples from the CON, NEC, and NEC+thEV groups, the same tissues used for histological analysis. Principal component analysis of the top 500 variable genes showed that the largest source of transcriptional variation (PC1, 50.8% of variance) distinctly separated CON groups from NEC and NEC+thEV groups (Fig. 1B). While the CON group clustered tightly, NEC and NEC+thEV groups were more dispersed, reflecting a shared injury-associated transcriptional program. Nonetheless, thMSC-EVs administration shifted the transcriptomic profile modestly toward the CON group, with the centroid distance to CON decreasing from 23.7 in the NEC group to 20.3 in the NEC+thEV group. At a single-gene level, a volcano plot identified marked upregulation of antimicrobial defense genes in the NEC group compared to the CON group, including as regenerating islet-derived protein 3 gamma and beta (*Reg3γ, Reg3β*), α-defensin (*Defa34*), group IIA phospholipase A2 (*Pla2g2a*), lysozyme

(*Lyz1*), and angiogenin (*Ang4*) (Fig. 1C, left panel). Of these, *Lyz1* and *Ang4* were significantly reduced in the NEC+thEV group compared to the NEC group, implying an attenuation of injury-associated antimicrobial response by thMSC-EV treatment (Fig. 1C, right panel). Consistent with these patterns, Gene Ontology biological process (GO BP) enrichment analysis showed that metabolic and catabolic processes predominated in the CON group, antimicrobial and antibacterial humoral responses in the NEC group, and catabolic and metabolic processes were partially restored in the NEC+thEV group (Fig. 1D). Together, these histological and transcriptomic findings indicated that thMSC-EVs treatment mitigates NEC-associated intestinal injury.

Proteomic comparison between naïve and thrombin-preconditioned MSC-derived EVs identified Annexin A1 as a candidate therapeutic mediator.

To determine the EV-derived therapeutic molecule that would underlie the protective effects of thMSC-EVs, we characterized their protein cargo by LC-MS/MS. Total protein analysis identified 4 proteins unique to naïveMSC-EVs, 71 unique to thMSC-EVs, and 1440 shared between the two (Fig. 2A). Of the 1440 shared proteins, 176 proteins were annotated as ligands in CellTalkDB, of which 109 were more abundant in thMSC-EVs than in naïveMSC-EVs. Together, these findings indicate that thrombin preconditioning does not substantially alter the composition of the EV cargo, but rather increases the abundance of existing cargo proteins. To identify which EV-derived ligand most strongly engages an injury-associated tissue receptor, we integrated the proteomic and transcriptomic datasets through annotated ligand–receptor pairs from CellTalkDB and computed an interaction score for each pair. The score combined the enrichment of ligands in thMSC-EVs relative to naïveMSC-EVs with the transcriptional induction of receptors in NEC relative to CON, thereby prioritizing interactions in which a thrombin-enriched EV ligand is matched to an injury-upregulated receptor. By this analysis, ANXA1–FPR1 emerged as the top-ranked interaction (Fig. 2B), consistent with confirmation of Annexin A1 3.8-fold more abundant in the thMSC-EVs compared to the naïveMSC-EVs (Fig. 2C).

We prioritized Annexin A1 for further evaluation, since its receptor signaling is known to engage with epithelial regeneration via Wnt/β-catenin signaling [40] and anti-inflammation [41], which has relevance of our interest to NEC recovery. Using KEGG pathway database, we identified that the downstream of Annexin A1 receptor converges on the TLR4-NF-kB pathway and Wnt/β-catenin pathways. Although the ANXA1–FPR2 pair, the classically known Annexin A1 receptor, received a lower interaction score than ANXA1–FPR1, which were 1.78 and 17.58 respectively, this difference reflected the constitutive expression of FPR2 irrespective of NEC induction. Given the marked enrichment of Annexin A1 in thMSC-EVs, its abundant delivery would be expected to engage both the injury-induced FPR1 and the constitutively available FPR2, potentially activating regenerative and tissue-protective signaling downstream of both receptors.

ANXA1 mediates the anti-apoptotic and anti-inflammatory effects of thMSC-EVs by inhibiting Akt pathway in in vitro NEC Models

To confirm the therapeutic effect of thMSC-EVs-derived Annexin A1, its mimetic peptide Ac2-26 was independently treated in an LPS-induced in vitro inflammatory model (Fig. 3A). The number of Ki67-positive cells, indicative of proliferating cells, was significantly reduced in the LPS group compared to the CON group. This count was significantly increased in the both LPS+thEV and LPS+Ac2-26 groups compared to the LPS group. While the mean count was lower in LPS+Ac2-26 group, there was no statistical difference compared to the LPS+thEV group, confirming Annexin A1-mediated proliferative effect. Similarly, the percentage of viable IEC-6 cells was significantly reduced in the LPS group compared to the CON group. Compared to the LPS group, the LPS + thEV and LPS + Ac2-26 groups showed a significant increase in cell viability. There were no significant differences between LPS + thEV and LPS + Ac2-26 groups.

The secretion of the pro-inflammatory cytokines IL-1α, IL-6, IL-1β, and TNF-α were measured using ELISA. Compared to the CON group, pro-inflammatory cytokines were significantly increased in the LPS group. IL-1α, IL-1β, and IL-6 were significantly reduced by both thMSC-EV and Ac2-26 treatment, whereas TNF-α showed a downward trend that did not reach statistical significance. The mean values of pro-inflammatory cytokines were greater in the LPS+Ac2-26 group, yet did not reach statistical significance.

To investigate the downstream signaling mechanisms by which Annexin A1 exerts its anti-apoptotic, proliferative, and anti-inflammatory effects, the Akt/NF-κB and Wnt/β-catenin pathways were examined by western blot (Fig. 4A). NF-κB expression was elevated in the LPS group compared with CON, and this increase was significantly attenuated in the LPS+thEV group and with a similar trend in the LPS+Ac2-26 group, indicating an anti-inflammatory response. β-catenin expression was significantly reduced in the LPS group relative to CON and was significantly restored in both the LPS+thEV and LPS+Ac2-26 groups, implying a reactivation of the regeneration-associated Wnt/β-catenin pathway. The level of Akt was significantly increased in the LPS group compared with CON and was significantly reduced in both the LPS+thEV and LPS+Ac2-26 groups, whereas phosphorylated Akt (p-Akt) was significantly decreased in the LPS group with only a non-significant trend toward recovery after treatment. Phosphorylated GSK3β levels did not differ significantly across groups, although it tended to decrease in the LPS group and increase in the LPS+thEV and LPS+Ac2-26 groups. Overall, these results suggest that Annexin A1 within thMSC-EVs suppresses the LPS-induced NF-κB pathway while restoring Wnt/β-catenin signaling, consistent with previously confirmed anti-inflammatory and proliferative effects.

Knockdown of Annexin A1 reduced the therapeutic efficacy of thMSC-EVs.

To confirm that Annexin A1 is essential for the therapeutic efficacy of thMSC-EVs, we knockdown Annexin A1 in MSCs by siRNA electroporation (si-thMSC-EVs) and isolated EVs from these cells for comparison with thMSC-EVs (Fig. 4B). Knockdown was confirmed at both mRNA and protein levels. Annexin A1 mRNA, western-blot, and ELISA all showed markedly reduced levels in the ANXA1-siRNA group relative to the scrambled-siRNA group. We then compared the therapeutic activity of sithMSC-EVs and thMSC-EVs in the LPS-induced inflammatory model (Fig. 4C). In the CCK-8 assay, LPS reduced cell viability relative to CON; both thMSC-EVs and si-thMSC-EVs significantly improved viability over LPS, but

si-thMSC-EVs was significantly less effective than thMSC-EVs, indicating a partial loss of the protective effect upon Annexin A1 knockdown. A similar pattern was observed for pro-inflammatory cytokines. LPS markedly elevated IL-1α, IL-1β, IL-6, and TNF-α, all of which were suppressed by thMSC-EVs. Knockdown of Annexin A1 attenuated this suppression. In IL-1β and TNF-α levels, si-thMSC-EVs yielded significantly higher cytokine levels than thMSC-EVs, whereas for IL-1α and IL-6 the suppression was statistically insignificant. This selective loss of efficacy suggests that Annexin A1 is a major but not exclusive effector of thMSC-EVs, with the retained suppression likely reflecting the contribution of other bioactive cargo within the EVs. Together, these reduced therapeutic efficacy suggests that Annexin A1 contributes substantially to the protective effects of thMSC-EVs.

Annexin A1 mediates the anti-inflammatory and integrity strengthening effects of thMSC-EVs in a multiple-stress HIT in vitro model.

To further assess the effect of Annexin A1 in multiple-stress HIT model, we assessed cell viability and the expression of ZO-1, a tight junction marker, using thMSC-EVs, Ac2-26, and si-thMSC-EVs. Percent cell viability was significantly reduced in the HIT group compared to the CON group, and was significantly increased in both the HIT+thEV and HIT+Ac2-26 groups compared to the HIT group. The protective effect of Ac2-26 was less than that of thMSC-EVs, yet was not statistically significant. Similarly, the expression level of ZO-1 was markedly reduced in the HIT group compared to the CON group, which was significantly restored in both the HIT+thEV and HIT+Ac2-26 groups compared to the HIT group. There was no significant difference between the two groups. These results indicate that Annexin A1 alone, delivered as the mimetic peptide Ac2-26, also recapitulated the cytoprotective and barrier-restoring effects of thMSC-EVs not only in the inflammatory model, but also in multiple gut injury HIT model.

Consistent results were obtained when comparing si-thMSC-EVs and thMSC-EVs (Fig. 5B). Cell viability was significantly reduced in the HIT group compared to the CON group, while both the HIT+thEV and HIT+siEV groups showed significantly increased viability compared to the HIT group. The viability of HIT+siEV group was significantly reduced compared to that of thMSC-EVs, suggesting a partial loss of efficacy upon Annexin A1 knockdown. The expression of ZO-1 was also markedly reduced in the HIT group compared to the CON group, and was significantly restored in both the HIT+thEV and HIT+siEV groups compared to the HIT group. There was no significant difference between HIT+thEV and HIT+siEV groups, yet the mean value was lower in the HIT+siEV group. These results suggested that Annexin A1 mediates the therapeutic efficacy of thMSC-EVs also in the multiple HIT model.

Discussion

In this study, we primarily demonstrated that Annexin A1 is the principal cargo molecule through which thMSC-EVs exert their therapeutic effect in experimental NEC. In vivo, thMSC-EVs reduced histological necrosis and epithelial apoptosis and partially reversed the injury-associated intestinal transcriptome, confirming the reproducibility of the benefit we reported previously [33]. Integrating the EV proteome with this injury-defined transcriptome nominated ANXA1-FPR1 as the most prominent ligand-receptor axis,

matching a thrombin-enriched cargo ligand to a receptor transcriptionally induced by injury. In vitro, the Annexin A1 mimetic peptide Ac2-26 delivered alone was sufficient to reproduce the pro-proliferative, cytoprotective, barrier-restoring, and anti-inflammatory effects of the intact vesicle across both an LPS-induced inflammatory model and a multiple-stress HIT model, while EVs depleted of Annexin A1 at source showed a significant loss of efficacy, establishing necessity. At the signaling level, both thMSC-EVs and Ac2-26 suppressed injury-induced NF-κB while restoring β-catenin expression, linking a single cargo protein to the two coupled arms of NEC pathology.

Necrotizing enterocolitis remains a devastating intestinal disease of preterm infants with limited therapeutic options. Building on our previous demonstration that thMSC-EVs ameliorate experimental NEC, the present study sought to identify the molecular mediator responsible for this benefit and to define its downstream mechanism. Whereas our previous study established that thMSC-EVs alleviate experimental NEC, the central challenge in EV research is to identify both what they contain and how they act. We hypothesized that combining the transcriptomics of the tissue after the thMSC-EVs administration and the proteomics of the thMSC-EVs' cargo would demonstrate answers to these two tasks. Through an integrated proteomic and transcriptomic analysis, we identified ANXA1–FPR axis as the mechanism by which thMSC-EVs exert the synergistic effect in ameliorating the key NEC pathophysiology: excessive inflammation and regeneration failure. The fundamental problem in NEC is the exaggerated immune response of the immature intestine to pathogen-associated molecular patterns (PAMPs) like LPS [15, 42, 43].

thMSC-EVs contain more than 1,400 proteins, and selecting a single therapeutic candidate among them was the first task of this study. Our previous study compared the abundance of these cargo proteins between naïveMSC-EVs and thMSC-EVs and presented the enriched GO terms, such as anti-apoptosis, anti-inflammation, cell adhesion, and Wnt signaling pathways [33]. Yet, comparing the abundance alone could not indicate which protein is relevant to the injured intestine, since a highly enriched cargo protein is not necessarily paired with a receptor available in the NEC gut. Conversely, the transcriptomics of the thMSC-EVs administered ileum presents the tissue's response but does not indicate which cargo protein elicited it. Therefore, to better identify the therapeutic mediator, we integrated the two datasets through the annotated ligand-receptor pairs, so that only the interactions in which a thrombin-enriched ligand meets an injury-induced receptor were prioritized. Notably, Annexin A1 was enriched 3.8-fold in thMSC-EVs, which is lower than that of other cargo proteins we previously reported, such as TIMP1, ITGB1, and THBS1 [33]. Annexin A1 was ranked first not because of its abundance within the EVs, but because its receptor was upregulated in the NEC intestine. To confirm whether Annexin A1 alone is sufficient, the mimetic peptide Ac2-26 was independently treated to the in vitro models, and to confirm whether it is necessary, EVs from Annexin A1-knockdown MSCs were compared with thMSC-EVs.

FPR2 is the classically described Annexin A1 receptor [44, 45], yet FPR1 received a markedly higher interaction score in our analysis. This is due to the scoring method rather than an evidence against FPR2 involvement, since the score involves receptors whose transcription is induced by injury, and FPR2 was constitutively expressed irrespective of NEC induction. Given the abundance of Annexin A1 delivered by

thMSC-EVs, engagement of both the injury-induced FPR1 and the constitutively available FPR2 is the most plausible interpretation. The relevance of FPR1 to the intestinal epithelium has been previously reported using a colitis model, that Annexin A1–containing EVs released from the intestinal epithelium accelerated mucosal wound healing in an FPR1-dependent manner, and that the delivery of the Ac2-26 peptide by polymeric nanoparticles reproduced this effect, similar to our study results [46]. Yet, our study differs that Annexin A1 was released from WJ-MSCs, and its abundance was increased by thrombin preconditioning. This suggests that the amount of Annexin A1 delivered can be controlled during the EV production process, which is an advantage for a manufactured therapeutic.

Annexin A1 was markedly enriched in thMSC-EVs relative to naïve EVs, and an unbiased ligand–receptor interaction analysis nominated the ANXA1–FPR1 axis as the most prominent injury-relevant interaction, matching a thrombin-enriched EV ligand to a receptor transcriptionally induced in the injured intestine. Furthermore, the Annexin A1 mimetic peptide Ac2-26, delivered on its own, reproduced the pro-proliferative, anti-apoptotic, and anti-inflammatory effects of thMSC-EVs across both an LPS-induced inflammatory model and a multiple-stress HIT model. ANXA1 significantly reduced pro-inflammatory cytokine secretion in peritoneal macrophages and significantly downregulated NF-kB, the key downstream transcription factor of the TLR4 signaling pathway[47, 48]. This anti-inflammatory action plausibly prevents secondary tissue damage from inflammation and creates a permissive environment necessary for cells to survive and begin regeneration [49–51].

A second and distinct role of Annexin A1 was regeneration. The Wnt/β-catenin signaling pathway is one of the most important regulators of the intestinal stem cell maintenance and the epithelial cell proliferation[20, 52]. In an inflammatory environment, this pathway is suppressed, preventing proper tissue repair [53]. In this study, both thMSC-EVs and Ac2-26 increased β-catenin expression, consistent with reactivation of Wnt signaling, which supports our previous confirmation that administration of thMSC-EVs increased intestinal stem cell markers in vivo and organoids [33, 54]. We therefore postulate that the intestinal stem cells were not merely stimulated to proliferate; they were first protected from the lethal inflammatory environment, which allowed them to fully exert their inherent regenerative potential [55, 56]. This sequencing remains a postulation, and therefore a further study using lineage tracing or crypt-specific reporter models is required.

Annexin A1 depletion significantly reduced therapeutic efficacy for cell viability and for IL-1β and TNF-α suppression, while the reductions for IL-1α and IL-6, though directionally consistent, did not reach significance. These consistent trends without statistical significance likely reflect small group sizes and the variability of injury models rather than an absence of effect. The consistent trend across multiple independent assays and models at molecular levels argues that Annexin A1 mediates the therapeutic effect of thMSC-EVs. It is notable that intact thMSC-EVs consistently produced greater efficacy than the Annexin A1 mimetic peptide alone, and that Annexin A1 knockdown reduced but did not completely abolish the therapeutic effect. Together, these findings indicate that Annexin A1 is a major but not exclusive effector of thMSC-EVs. This is consistent with the nature of EVs as multi-component delivery vehicles. Beyond Annexin A1, thMSC-EVs carry a diverse repertoire of proteins, lipids, and nucleic acids,

many of which possess independent cytoprotective, anti-inflammatory, or regenerative activities [57]. The retained efficacy of Annexin A1–knockdown EVs reflects the contribution of these additional bioactive cargoes acting in parallel with, or in addition to, Annexin A1. In our previous proteomic comparison, THBS1, TIMP1, ITGB1, and FGF2 were each enriched more than five-fold in thMSC-EVs and carry anti-apoptotic, cell adhesion, or Wnt-associated annotations that could plausibly account for the residual effect [33]. This multi-factorial composition provides a mechanistic rationale for why the intact EV offer advantages over a single purified molecule as a therapeutic strategy.

Recent studies have revealed that ANXA1 exerts similar anti-inflammatory and tissue-protective actions across a variety of inflammatory and necrotic disease models, including rheumatoid arthritis, atherosclerosis, ischemic stroke, and tissue injury [58–60]. In these contexts, ANXA1 commonly attenuated excessive immune responses through the inhibition of NF-κB signaling and modulation of macrophage polarization toward an M2 reparative phenotype [61, 62]. These mechanisms closely parallel our findings in the NEC model, in which thMSC-EVs, enriched in ANXA1, not only suppress inflammation but also facilitate regeneration by stabilizing the Wnt/β-catenin pathway and supporting intestinal stem cell survival. This offers an explanation for the reproducible efficacy of thMSC-EVs across brain, lung, and gut neonatal injury models [33–36]. ANXA1-FPR signaling converging on anti-inflammation and repair irrespective of tissue may underlie benefits across different disease models. Therefore, our results strengthen the concept that ANXA1-driven pathways represent a convergent strategy for resolving pathological inflammation and promoting repair in diverse disease states. This broader relevance underscores the therapeutic potential of targeting ANXA1, either by mimetic peptides or EV-based delivery, for a spectrum of conditions characterized by inflammation and tissue damage, extending beyond NEC to other refractory inflammatory and necrotic diseases.

Because Annexin A1 has been identified as a key therapeutic effector, it may serve as a reference marker for quality control (QC) and potency assays addressing batch-to-batch variability of thMSC-EVs. Towards the production of GMP-grade thMSC-EVs, QC and potency assays using ANXA1 could provide a quantifiable release criterion linked to a defined mechanism of action, rather than to particle count alone, which is the goal of MISEV [29]. This is a critical step in the standardization and regulatory approval process for complex biological drugs.

This study has several limitations. First, the EV proteomic comparison was performed without replicates. Second, the transcriptomic analysis was performed on a modest number of animals per group, which limited statistical power for individual genes and pathways and precluded detection of subtle treatment effects. Third, the ligand–receptor analysis required ortholog-based mapping of the human EV proteome onto mouse gene symbols before comparison against mouse-native ligand–receptor annotations. No database currently maps ligand-receptor interactions across species directly. Lastly, the mechanistic signaling experiments were conducted in vitro, due to the limited availability of EVs, and therefore in vivo confirmation remains as the most important next step. For the translation of these findings into clinical applications, further preclinical investigations are needed to determine the optimal timing, dosage, and route of administration of thMSC-EVs. Finally, incorporating additional analyses such as miRNA profiling

and lipidomics would allow for a more holistic understanding of thMSC-EVs. These approaches could elucidate how not only proteins but also microRNAs, metabolites, and lipid constituents interact with ANXA1, TIMP1, FGF2, and related molecules to mediate the observed therapeutic effects. Such integrative studies may yield valuable insights for identifying novel biomarkers and developing combinatorial strategies to maximize the therapeutic efficacy of thMSC-EVs.

In conclusion, our findings identified Annexin A1 as a key mediator of the therapeutic efficacy of thrombin-preconditioned MSC-derived EVs in experimental NEC, acting through suppression of NF-κB–driven inflammation and restoration of regeneration-associated β-catenin signaling. An integrative proteomic and transcriptomic strategy discovered the ANXA1-FPR axis from among diverse cargo proteins. The mimetic peptide Ac2-26 established that Annexin A1 is sufficient to reproduce the protective phenotype, and Annexin A1-depleted EVs established that it is necessary for full efficacy. While Annexin A1 alone reproduces much of the protective phenotype, the superior and more complete efficacy of intact thMSC-EVs underscores the therapeutic value of their diverse molecular cargo. These results support Annexin A1–enriched, thrombin-preconditioned EVs as a promising cell-free therapeutic strategy for NEC and provide a mechanistic foundation for their further development, as well as a defined potency marker for their clinical-grade manufacture.

Declarations

Ethics approval and consent to participate

All procedures involving human cells and animals were reviewed and approved by the institution. Human Wharton's Jelly-derived MSCs (WJ-MSCs) were obtained from the Samsung Medical Center's Good Manufacturing Practice (GMP) Facility. The obtained WJ-MSCs was established from a single donor with informed consent under Samsung Medical Center’s Institutional Review Board (IRB) approval (IRB approval number: 2016-07-102-043; Date of approval: 2016-09-20; Approval expiration date: 2025-09-15; Study name: Study on the Selection of Optimal Mesenchymal Stem Cells from Different Sources for the Treatment of Chronic/Intractable Diseases including Alzheimer's Disease and Musculoskeletal Disorders). The Institutional Animal Care and Use Committee (IACUC) of the Research Institute for Future Medicine (RIFM) at Samsung Medical Center approved all animal protocols (No. 20231115001, No. 20230116001; Approval Date: 2023.12.22 and 2023.02.22; Study name: Evaluation of the therapeutic efficacy of Wharton’s jelly-derived mesenchymal stromal cell-derived extracellular vesicles on neonatal necrotizing enterocolitis experimental model). The RIFM is an AAALAC International-accredited institution, and all animal care followed the Institute of Laboratory Animal Resources guide. The animal study was performed in accordance with ARRIVE guidelines, and euthanasia was conducted following the 2020 AVMA Guidelines. All studies were conducted within the study period indicated in the IRB.

Conflict of interests

The funders had no role in the study design; collection, analyses, or interpretation of data; writing of the manuscript; or decision to publish the results. Yun Sil Chang, Sein Hwang, Chol Eun Kwon, and Young

Eun Kim declare potential conflicts of interest arising from an issued patent titled "AnnexinA1 protein or functional fragment thereof for use in the treatment of necrotizing enterocolitis (10-2026-0013567)" as co-inventors, not as patentees.

Funding

This research was supported by a grant from the Korea Health Technology R&D Project through the Korea Health Industry Development Institute (KHIDI), funded by the Ministry of Health & Welfare, Republic of Korea (KH129441 and RS-2024-00436750); by the Korean Fund for Regenerative Medicine (KFRM) grant funded by the Korean government (Ministry of Science and ICT, Ministry of Health & Welfare) (23C0119L1).

Author Contribution

C.E.K and S.H contributed to Formal analysis, Investigation, Methodology, and Writing-original draftY.E.K, M.Y, and S.Y.A contributed to InvestigationS.I.S contributed to Conceptualization, Investigation, Writing-original draft, Funding acquisitionY.S.C contributed to Conceptualization, Investigation, Writing- review & editing, Funding acquisition, Supervision, Corresponding author

All authors reviewed the manuscript.

Acknowledgements

The authors used AI assistance for grammar checking and readability improvement. The tool was not used to generate original data. The authors reviewed and approved the final text.

Availability of data and materials

The raw RNA-seq dataset supporting the conclusions of this article is available in the Zenodo repository, [DOI: 10.5281/zenodo.23166023].

References

1. Alsaied A, Islam N, Thalib L. Global incidence of Necrotizing Enterocolitis: a systematic review and Meta-analysis. BMC Pediatr. 2020;20(1):344.
2. Yee WH, et al. Incidence and timing of presentation of necrotizing enterocolitis in preterm infants. Pediatrics. 2012;129(2):e298–304.
3. Mekonnen SM, et al. The Prevalence of Necrotizing Enterocolitis and Associated Factors Among Enteral Fed Preterm and Low Birth Weight Neonates Admitted in Selected Public Hospitals in Addis

Ababa, Ethiopia: A Cross-sectional Study. Glob Pediatr Health. 2021;8:2333794X211019695.

4. Patel BK, Shah JS. *Necrotizing enterocolitis in very low birth weight infants: a systemic review.* ISRN Gastroenterol, 2012. 2012: p. 562594.
5. Shulhan J, et al. Current Knowledge of Necrotizing Enterocolitis in Preterm Infants and the Impact of Different Types of Enteral Nutrition Products. Adv Nutr. 2017;8(1):80–91.
6. Jones IH, Hall NJ. Contemporary Outcomes for Infants with Necrotizing Enterocolitis-A Systematic Review. J Pediatr. 2020;220:86–e923.
7. Fitzgibbons SC, et al. Mortality of necrotizing enterocolitis expressed by birth weight categories. J Pediatr Surg. 2009;44(6):1072–5. discussion 1075–6.
8. Battersby C, et al. Incidence and enteral feed antecedents of severe neonatal necrotising enterocolitis across neonatal networks in England, 2012-13: a whole-population surveillance study. Lancet Gastroenterol Hepatol. 2017;2(1):43–51.
9. Nino DF, Sodhi CP, Hackam DJ. Necrotizing enterocolitis: new insights into pathogenesis and mechanisms. Nat Rev Gastroenterol Hepatol. 2016;13(10):590–600.
10. Kasivajjula H, Maheshwari A. Pathophysiology and current management of necrotizing enterocolitis. Indian J Pediatr. 2014;81(5):489–97.
11. Kandasamy J, et al. Inflammatory signals that regulate intestinal epithelial renewal, differentiation, migration and cell death: Implications for necrotizing enterocolitis. Pathophysiology. 2014;21(1):67–80.
12. Li B, et al. Exploring the Complex Pathophysiology of Necrotizing Enterocolitis in Preterm Neonates. Annu Rev Pathol. 2026;21(1):37–58.
13. Mihi B, et al. Interleukin-22 signaling attenuates necrotizing enterocolitis by promoting epithelial cell regeneration. Cell Rep Med. 2021;2(6):100320.
14. Hunter CJ, De Plaen IG. Inflammatory signaling in NEC: Role of NF-kappaB, cytokines and other inflammatory mediators. Pathophysiology. 2014;21(1):55–65.
15. Mihi B, Good M. Impact of Toll-Like Receptor 4 Signaling in Necrotizing Enterocolitis: The State of the Science. Clin Perinatol. 2019;46(1):145–57.
16. Sodhi CP, et al. Toll-like receptor-4 inhibits enterocyte proliferation via impaired beta-catenin signaling in necrotizing enterocolitis. Gastroenterology. 2010;138(1):185–96.
17. Ishiyama A et al. Necrotizing Enterocolitis: A Comprehensive Review on Toll-like Receptor 4-Mediated Pathophysiology, Clinical, and Therapeutic Insights. Biomedicines, 2025. 13(9).
18. Li B, et al. Impaired Wnt/beta-catenin pathway leads to dysfunction of intestinal regeneration during necrotizing enterocolitis. Cell Death Dis. 2019;10(10):743.
19. Gomart A, Vallee A, Lecarpentier Y. Necrotizing Enterocolitis: LPS/TLR4-Induced Crosstalk Between Canonical TGF-beta/Wnt/beta-Catenin Pathways and PPARgamma. Front Pediatr. 2021;9:713344.
20. Fevr T, et al. Wnt/beta-catenin is essential for intestinal homeostasis and maintenance of intestinal stem cells. Mol Cell Biol. 2007;27(21):7551–9.

21. Villamor-Martinez E, et al. Stem Cells as Therapy for Necrotizing Enterocolitis: A Systematic Review and Meta-Analysis of Preclinical Studies. Front Pediatr. 2020;8:578984.
22. Tayman C, et al. Mesenchymal stem cell therapy in necrotizing enterocolitis: a rat study. Pediatr Res. 2011;70(5):489–94.
23. Yang J, et al. Heparin-binding epidermal growth factor-like growth factor and mesenchymal stem cells act synergistically to prevent experimental necrotizing enterocolitis. J Am Coll Surg. 2012;215(4):534–45.
24. Zani A, et al. Amniotic fluid stem cells improve survival and enhance repair of damaged intestine in necrotising enterocolitis via a COX-2 dependent mechanism. Gut. 2014;63(2):300–9.
25. McCulloh CJ, et al. Evaluating the efficacy of different types of stem cells in preserving gut barrier function in necrotizing enterocolitis. J Surg Res. 2017;214:278–85.
26. McCulloh CJ, et al. Treatment of experimental necrotizing enterocolitis with stem cell-derived exosomes. J Pediatr Surg. 2018;53(6):1215–20.
27. Weis VG, et al. Human placental-derived stem cell therapy ameliorates experimental necrotizing enterocolitis. Am J Physiol Gastrointest Liver Physiol. 2021;320(4):G658–74.
28. Baek G, et al. Mesenchymal Stem Cell-Derived Extracellular Vesicles as Therapeutics and as a Drug Delivery Platform. Stem Cells Transl Med. 2019;8(9):880–6.
29. Welsh JA, et al. Minimal information for studies of extracellular vesicles (MISEV2023): From basic to advanced approaches. J Extracell Vesicles. 2024;13(2):e12404.
30. Sung DK et al. Thrombin Preconditioning of Extracellular Vesicles Derived from Mesenchymal Stem Cells Accelerates Cutaneous Wound Healing by Boosting Their Biogenesis and Enriching Cargo Content. J Clin Med, 2019. 8(4).
31. Ocansey DKW, et al. Improved therapeutics of modified mesenchymal stem cells: an update. J Transl Med. 2020;18(1):42.
32. Noronha NC, et al. Priming approaches to improve the efficacy of mesenchymal stromal cell-based therapies. Stem Cell Res Ther. 2019;10(1):131.
33. Hwang S, et al. Thrombin-preconditioned mesenchymal stromal cell-derived extracellular vesicles attenuate experimental necrotizing enterocolitis. Stem Cell Res Ther. 2025;16(1):101.
34. Ahn SY, et al. Vascular endothelial growth factor mediates the therapeutic efficacy of mesenchymal stem cell-derived extracellular vesicles against neonatal hyperoxic lung injury. Exp Mol Med. 2018;50(4):1–12.
35. Kim YE et al. Mesenchymal-Stem-Cell-Derived Extracellular Vesicles Attenuate Brain Injury in Escherichia coli Meningitis in Newborn Rats. Life (Basel), 2022. 12(7).
36. Kim YE et al. Thrombin Preconditioning Enhances Therapeutic Efficacy of Human Wharton's Jelly-Derived Mesenchymal Stem Cells in Severe Neonatal Hypoxic Ischemic Encephalopathy. Int J Mol Sci, 2019. 20(10).

37. Shao X et al. CellTalkDB: a manually curated database of ligand-receptor interactions in humans and mice. Brief Bioinform, 2021. 22(4).
38. Zani A, et al. Assessment of a neonatal rat model of necrotizing enterocolitis. Eur J Pediatr Surg. 2008;18(6):423–6.
39. Jin S, et al. Inference and analysis of cell-cell communication using CellChat. Nat Commun. 2021;12(1):1088.
40. Rubinstein MR et al. Fusobacterium nucleatum promotes colorectal cancer by inducing Wnt/beta-catenin modulator Annexin A1. EMBO Rep, 2019. 20(4).
41. Han PF, et al. Annexin A1 involved in the regulation of inflammation and cell signaling pathways. Chin J Traumatol. 2020;23(2):96–101.
42. Broering MF, et al. Development of an Inflamed High Throughput Stem-cell-based Gut Epithelium Model to Assess the Impact of Annexin A1. Stem Cell Rev Rep. 2024;20(5):1299–310.
43. Hackam DJ et al. *Innate immune signaling in the pathogenesis of necrotizing enterocolitis.* Clin Dev Immunol, 2013. 2013: p. 475415.
44. Xu X, et al. Annexin A1 protects against cerebral ischemia-reperfusion injury by modulating microglia/macrophage polarization via FPR2/ALX-dependent AMPK-mTOR pathway. J Neuroinflammation. 2021;18(1):119.
45. Bena S, et al. Annexin A1 interaction with the FPR2/ALX receptor: identification of distinct domains and downstream associated signaling. J Biol Chem. 2012;287(29):24690–7.
46. Leoni G, et al. Annexin A1-containing extracellular vesicles and polymeric nanoparticles promote epithelial wound repair. J Clin Invest. 2015;125(3):1215–27.
47. Zhang G, Ghosh S. Toll-like receptor-mediated NF-kappaB activation: a phylogenetically conserved paradigm in innate immunity. J Clin Invest. 2001;107(1):13–9.
48. Zhao Y, et al. Decoding nature: multi-target anti-inflammatory mechanisms of natural products in the TLR4/NF-kappaB pathway. Front Pharmacol. 2024;15:1467193.
49. Sugimoto MA et al. *Annexin A1 and the Resolution of Inflammation: Modulation of Neutrophil Recruitment, Apoptosis, and Clearance.* J Immunol Res, 2016. 2016: p. 8239258.
50. McArthur S, et al. Annexin A1 drives macrophage skewing to accelerate muscle regeneration through AMPK activation. J Clin Invest. 2020;130(3):1156–67.
51. Alhasan H, et al. Inhibitory role of Annexin A1 in pathological bone resorption and therapeutic implications in periprosthetic osteolysis. Nat Commun. 2022;13(1):3919.
52. Sun H et al. Wnt/beta-catenin signaling within multiple cell types dependent upon kramer regulates Drosophila intestinal stem cell proliferation. bioRxiv, 2023.
53. Kretzschmar K, Clevers H. Wnt/beta-catenin signaling in adult mammalian epithelial stem cells. Dev Biol. 2017;428(2):273–82.
54. Hageman JH, et al. Intestinal Regeneration: Regulation by the Microenvironment. Dev Cell. 2020;54(4):435–46.

55. Umar S. Intestinal stem cells. Curr Gastroenterol Rep. 2010;12(5):340–8.
56. Choi J, Augenlicht LH. Intestinal stem cells: guardians of homeostasis in health and aging amid environmental challenges. Exp Mol Med. 2024;56(3):495–500.
57. Hwang S et al. Extracellular vesicles from mesenchymal stromal cells: an emerging therapy for intractable neonatal disorders. Stem Cells Transl Med, 2025. 14(10).
58. Qian Z, et al. Annexin A: Cell Death, Inflammation, and Translational Medicine. J Inflamm Res. 2025;18:5655–72.
59. McArthur S, et al. Annexin A1: a central player in the anti-inflammatory and neuroprotective role of microglia. J Immunol. 2010;185(10):6317–28.
60. Kelly L, et al. Annexin-A1: The culprit or the solution? Immunology. 2022;166(1):2–16.
61. Zhang Z, et al. Annexin 1 induced by anti-inflammatory drugs binds to NF-kappaB and inhibits its activation: anticancer effects in vitro and in vivo. Cancer Res. 2010;70(6):2379–88.
62. Moraes LA, et al. Annexin-A1 enhances breast cancer growth and migration by promoting alternative macrophage polarization in the tumour microenvironment. Sci Rep. 2017;7(1):17925.

Figures

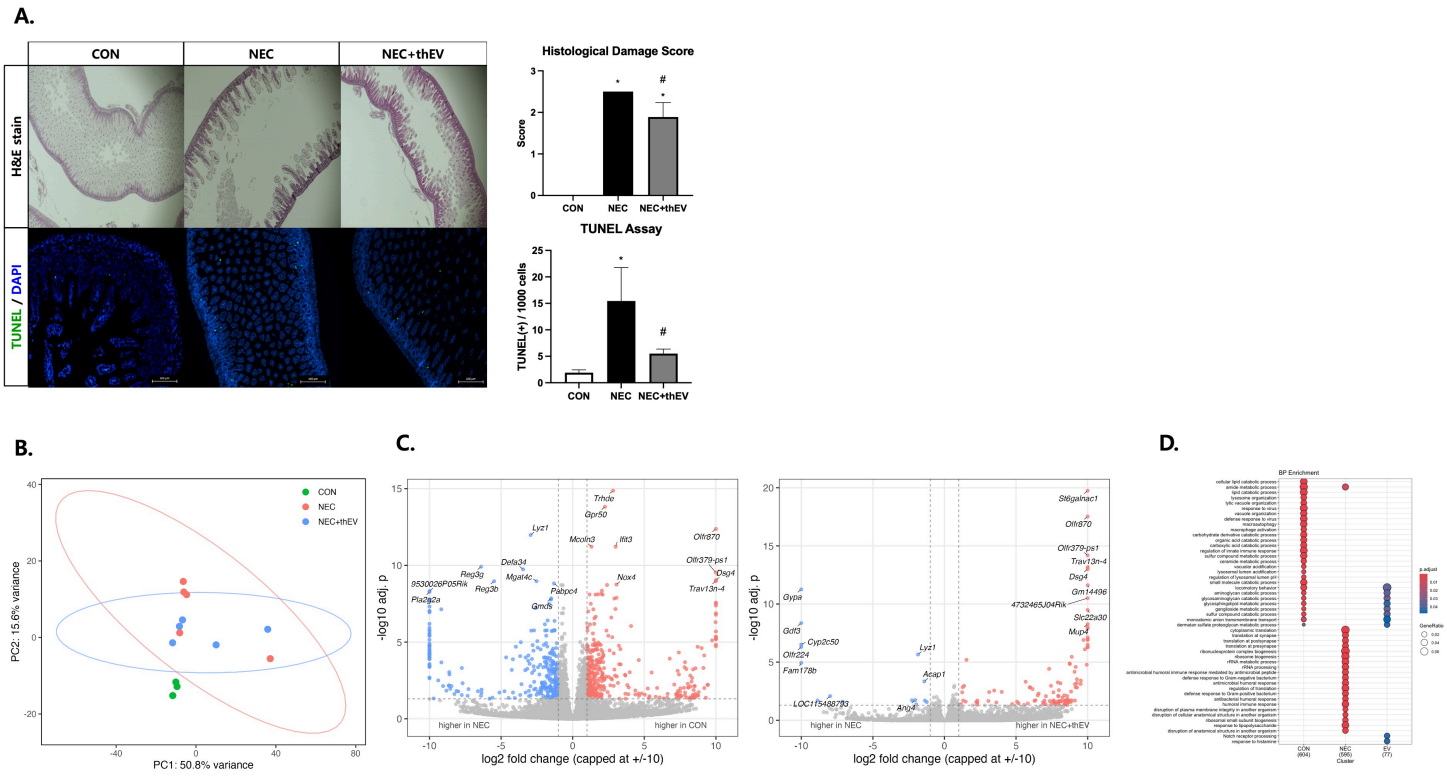


Figure 1

(A) Representative images of H&E staining and TUNEL assay of ileal tissues from CON, NEC, and NEC+thEV groups. One-way ANOVA and the post-hoc Tukey test were used. *p<0.05 vs. CON; #p<0.05 vs. NEC. n= 6, 6, 6 / groups. **(B)** PCA of the top 500 variable genes from the in vivo ileal sample bulk-seq. Each point represents one animal. The first two principal components account for 50.8% (PC1) and 15.6% (PC2) of the total variance. The Euclidean distance between group centroids in PC1–PC2 space was 23.7 between CON and NEC groups, and 20.3 between CON and NEC+thEV groups. n=3,5,5/groups. **(C)** Volcano plot representation of differentially expressed genes between the CON and NEC groups (left) and between the NEC and NEC+thEV groups (right). **(D)** Bubble plot representation of the Gene Ontology biological processes enriched in each group. The color of the bubble represents the adjusted p-value and the size represents the gene ratio. Data are presented as mean±SEM. CON, normal control; NEC, necrotizing enterocolitis control group; NEC+thEV, thMSC-EVs treated NEC group; thMSC-EVs, thrombin-preconditioned MSC-derived EVs; PC, principal component;

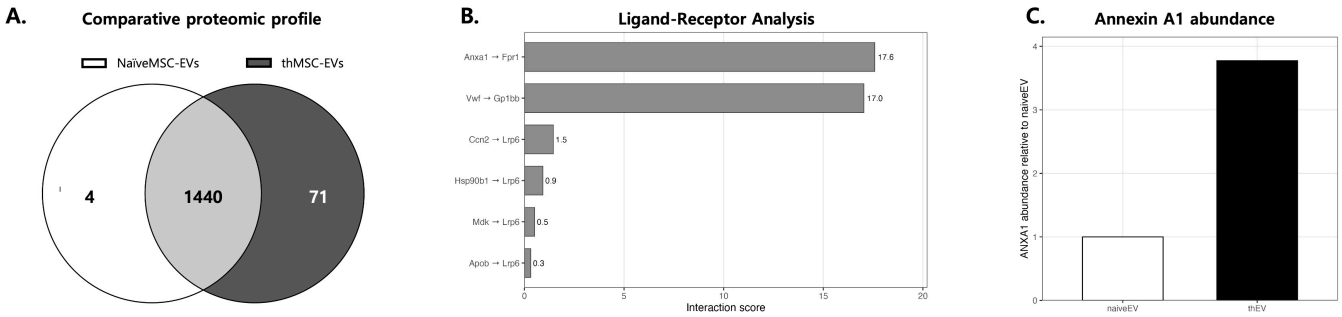


Figure 2

(A) Venn diagram of the proteins detected in naïveMSC-EVs and thMSC-EVs by LC-MS/MS. **(B)** Bar graph representation of the interaction scores of the ligand–receptor pairs identified by integrating the thMSC-EV proteome with the NEC ileal transcriptome. The interaction score was calculated as ligand log2 fold change (thEV/naïveEV) × receptor log2 fold change (NEC/CON), and the value of each pair is presented to the right of the bar. **(C)** Bar graph representation of the abundance of Annexin A1 in thMSC-EVs relative to that in naïveMSC-EVs. naïveMSC-EVs, naïve MSC-derived EVs; thMSC-EVs, thrombin-

preconditioned MSC-derived EVs; ANXA1, Annexin A1; FPR1, formyl peptide receptor 1; LC-MS/MS, liquid chromatography with tandem mass spectrometry

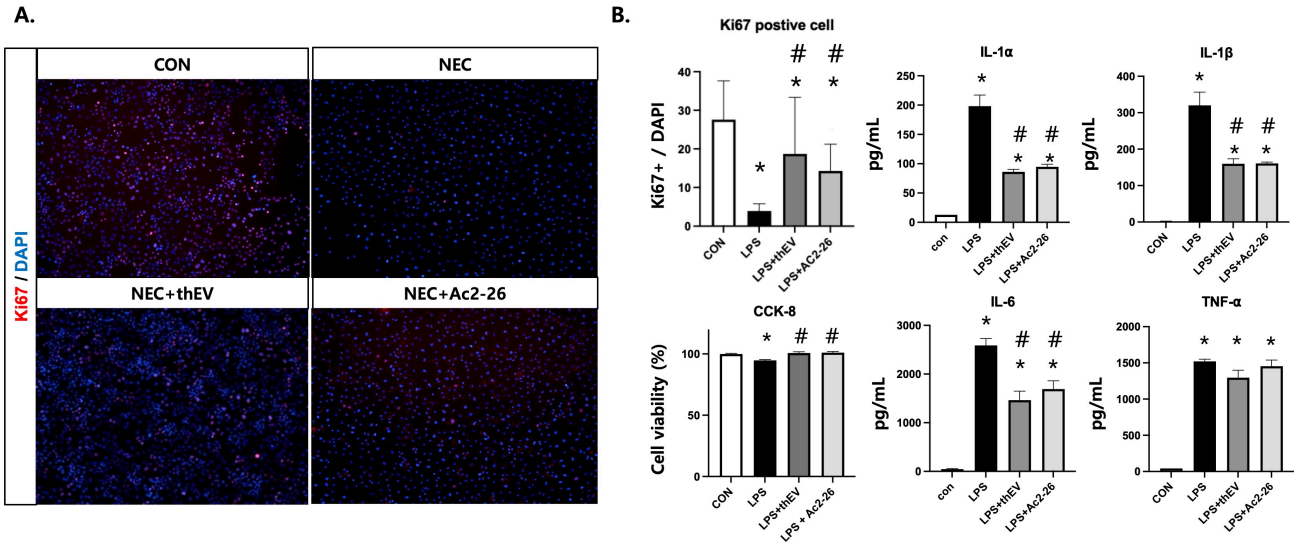


Figure 3

(A) Representative microscopic images of immunocytochemically stained Ki67 (+) cells counterstained with DAPI. **(B)** Bar graph representation of the quantification of Ki67 (+) cells normalized to DAPI, the CCK-8 cell viability assay, and the levels of pro-inflammatory cytokines IL-1α, IL-1β, IL-6, and TNF-α measured using ELISA. n = 20,20,20,20 per CON, LPS, LPS+thEV, and LPS+Ac2-26 groups, respectively. *, $p < 0.05$ vs. CON; #, $p < 0.05$ vs. LPS; $, $p < 0.05$ vs. LPS+thEV. Data are presented as mean±SEM. One-way ANOVA and the post-hoc Tukey test were used in the analysis. CON, normal control; LPS, lipopolysaccharide; LPS+thEV, thMSC-EVs treated LPS group; LPS+Ac2-26, Annexin A1 mimetic peptide treated LPS group; IL, interleukin; TNF, tumor necrosis factor;

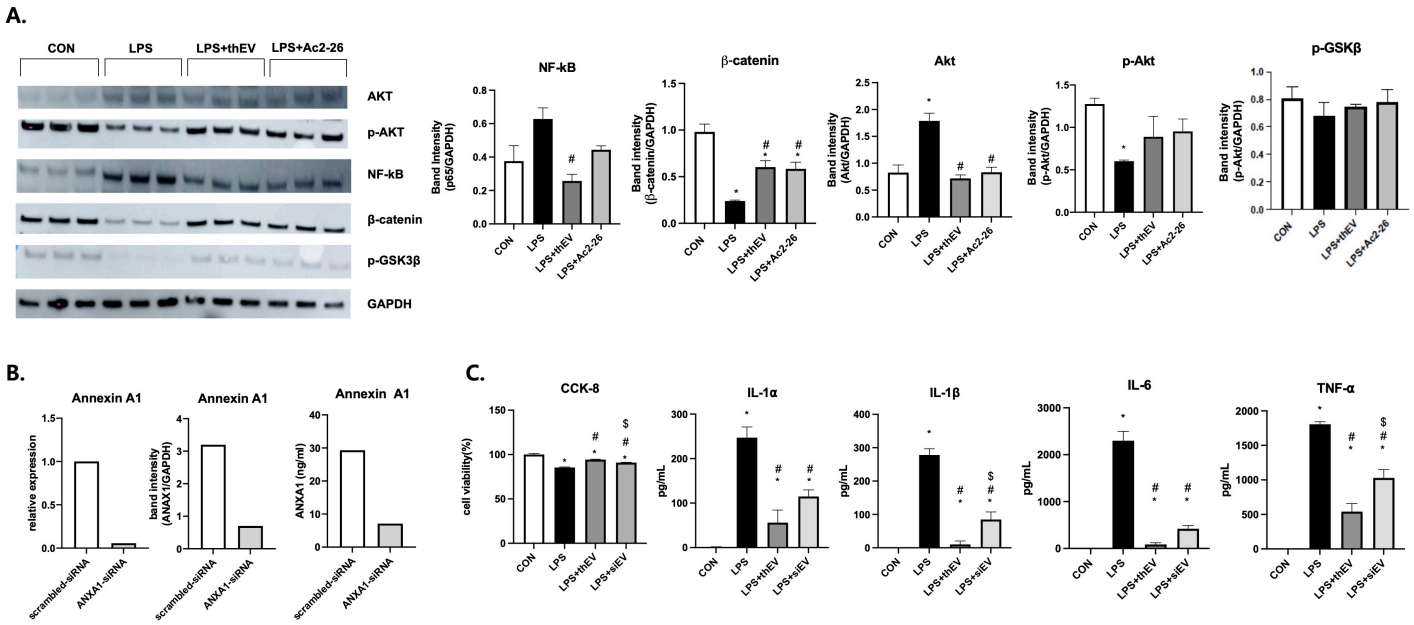


Figure 4

(A) Representative western blot images and bar graph representation of the protein expression levels of AKT, p-AKT, NF-κB, β-catenin, and p-GSK3β normalized to GAPDH in IEC-6 cells. n = 20,20,20,20 in the CON, LPS, LPS+thEV, and LPS+Ac2-26 groups, respectively. *, $p < 0.05$ vs. CON; #, $p < 0.05$ vs. LPS. **(B)** Bar graph representation of the confirmation of Annexin A1 knockdown in WJ-MSCs, showing the relative mRNA expression analyzed via RT-qPCR, the band intensity normalized to GAPDH analyzed via western blot, and the protein concentration measured using ELISA. n = 5,5 per scrambled-siRNA and ANXA1-siRNA groups, respectively. **(C)** Bar graph representation of the CCK-8 cell viability assay and the levels of pro-inflammatory cytokines IL-1α, IL-1β, IL-6, and TNF-α measured using ELISA. n = 20,20,20,20 in the CON, LPS, LPS+thEV, and LPS+siEV groups, respectively. *, $p < 0.05$ vs. CON; #, $p< 0.05$ vs. LPS; $, $p < 0.05$ vs. LPS+thEV. Data are presented as mean±SEM. One-way ANOVA and the post-hoc Tukey test were used in the analysis. LPS+siEV, ANXA1-knockdown thMSC-EVs treated LPS group; ANXA1, Annexin A1; WJ-MSCs, Wharton's jelly-derived mesenchymal stromal cells; RT-qPCR, real-time quantitative polymerase chain reaction

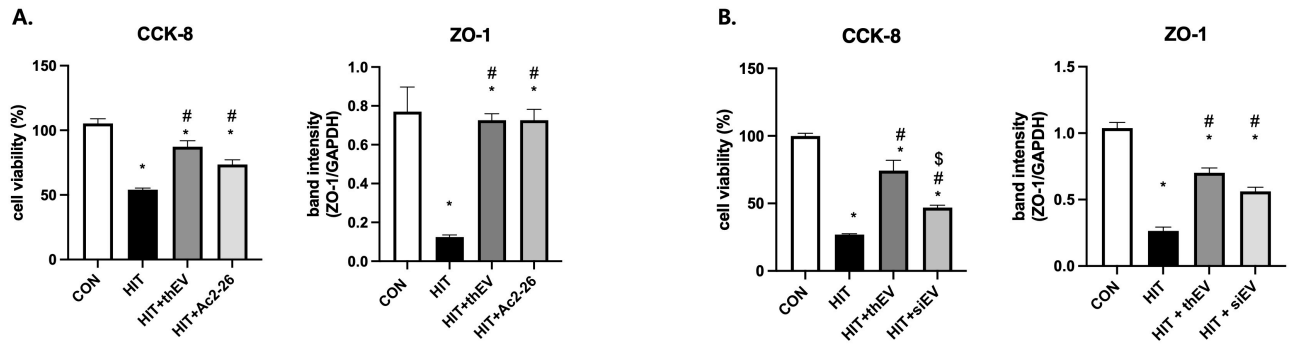


Figure 5

(A) Bar graph representation of the CCK-8 cell viability assay and the western blot protein expression levels of ZO-1 normalized to GAPDH in IEC-6 cells. n = 8,8,8,8 in the CON, HIT, HIT+thEV, and HIT+Ac2-26 groups, respectively. **(B)** Bar graph representation of the CCK-8 cell viability assay and the western blot protein expression levels of ZO-1 normalized to GAPDH in IEC-6 cells. n = 8,8,8,8 in the CON, HIT, HIT+thEV, and HIT+siEV groups, respectively. *, $p < 0.05$ vs. CON; #, $p < 0.05$ vs. HIT; $, $p < 0.05$ vs. HIT+thEV. Data are presented as mean±SEM. One-way ANOVA and the post-hoc Tukey test were used in the analysis. HIT, hyperosmolar stress, ischemia, and hypothermia-induced IEC-6 cells; HIT+thEV, thMSC-EVs treated HIT group; HIT+Ac2-26, Annexin A1 mimetic peptide treated HIT group; HIT+siEV, ANXA1-knockdown thMSC-EVs treated HIT group; ZO-1, zonula occludens-1

Supplementary Files

This is a list of supplementary files associated with this preprint. Click to download.

- SupplementaryFigureFullblot.jpg